Systematic study on FRET-pair functionalization of mesoporous thin films for correlation of pH-sensing and ionic mesopore accessibility

Mathias Stanzel[a], Robert Brilmayer[a], Markus Langhans[b], Tobias Meckel[b], Annette Andrieu-Brunsen[a]*

[a]*Ernst-Berl Institut für Technische und Makromolekulare Chemie, Technische Universität Darmstadt, Alarich-Weiss-Strasse 4,D-64287 Darmstadt, Germany*

[b]*Membrane Dynamics, Department of Biology, Technische Universität Darmstadt, Schnittspahnstraße 3-5, 64287, Darmstadt, Germany*

*Corresponding author. Tel.: +49-6151-16-23742.
E-mail address: andrieu-brunsen@smartmem.tu-darmstadt.de.

Abstract

Ordered mesoporous silica materials (OMS) are relevant in various applications such as separation, catalysis, or drug delivery. Thereby their performance is mainly dependent on mesopore accessibility and molecular transport within mesopores which is strongly influenced by the spatial confinement. This is especially relevant in case of charged mesopore walls and thus electrostatically controlled transport. Therefore, it is highly important to monitor charged states of functionalized mesopores. In this study we adapt pH-probing strategies, known from pH-monitoring e.g. in cells, to mesoporous thin films aiming to monitor mesopore charge and correlate this to mesopores ionic permselectivity. Therefore, grafting of a FRET dye pair, consisting of a pH-sensitive dye (fluorescein isothiocyanate (FITC)) and a pH-insensitive reference dye (rhodamine B isothiocyanate (RITC)), to the mesopore wall is optimized. The grafted FITC-RITC FRET pair allows to monitor mesopore "pH" over a broad range of up to six pH-units after optimization of FRET pair functionalization. Thereby, "pH" monitoring is performed based on absorption and fluorescence readout using confocal microscopy baring the potential of localized detection. The detected pH-dependent absorption and fluorescence emission is in good agreement with the pH-dependent ionic mesopore permselectivity, and thus with the influence of mesopore confinement on ionic permselectivity as detected by cyclic voltammetry. In addition, this study not only shows the possibility of using FRET dye pairs for monitoring charged states in mesopores but as well the influence of these probing dye molecules on the mesopores characteristics, such as ionic permselectivity, indicating the need of optimizing functionalization with probe molecules.

Keywords: mesoporous thin films, pH-detection, confinement effects, FRET dye pair, ionic permselectivity, ionic mesopore accessibility

1. Introduction

Ordered mesoporous silica (OMS) present high specific surface area and structural stability while offering tunable pore sizes and geometries [1, 2]. Due to the high number of surface silanol groups, OMS can be modified with a variety of organic functional groups [3, 4]. The broad range of functionalization opportunities together with their tunable pore structure and material architecture are main reasons for OMS having attracted significant research interest and a variety of applications such as controlled drug release [5], microfluidic devices, sensing [6], lab-on-chip devices [1, 7-10], bioseparation [11, 12], drug delivery [13, 14], oil production [15], oil-water separation or proton transport [11, 16-18], e.g. in the context of energy conversion have been proposed over the last decades. Changing solution pH and thus charge density in nanopores directly affects mesopore accessibility and transport and thus the mentioned applications. Thereby, pore size as well as pore wall functional group- and thus charge density, affect "pH" within mesopores. It has been demonstrated, that mesopore "pH" might strongly differ from the measurable solution pH [3, 19-22].

Inspired by natural ion channels and -pores, systematic investigation of polymer functionalization in spatially confined mesopores [23-25] within the last years resulted in a plethora of functionalized mesopores with adjustable pore accessibility and ionic transport mainly using electrostatic interaction. Gating of ionic transport as well as gradual tuning of mesopore accessibility have been achieved by incorporation of stimuli responsive functional units, often polymers, reacting to stimuli such as solution pH, potential, or light. [10, 26-34] More recently, controlling polymer amount and thus charge density inside mesopores has resulted in gradual variation of ionic mesopores accessibility. [23-25, 35] In case of pH-gated or gradually tuned ionic mesopore accessibility only the solution pH can be adjusted. The "pH" within the mesopores remains often unknown and cannot be directly monitored experimentally. In this context, only a few studies tried to correlate the resulting ionic permselectivity with gradual solution pH-changes. Doing so a difference between the measured solution pH and the expected pK_a-controlled ionic permselectivity has been observed [22]. Only after considering the influence of the spatial confinement and proximity of generated mesopore wall charges, the experimental titration curve could be theoretically reproduced [36]. Such nanoscale confinement effects on charge density and protonation-deprotonation equilibria are as well reported for hydrogels [37, 38], and concave nanoparticles

for which curvature plays a role [39]. This shows the need for experimental strategies to directly monitor the "pH" in spatially confined nanopores which are still missing to date. In this context, strategies enabling "pH" monitoring in mesopores, ideally with spatiotemporal control, bare the potential to directly monitor mesoporous charged states, as e.g. in smart porous materials with switchable charge density or charge density gradients. In addition, fluorescence detection bares the potential to go towards localized detection, potentially down to single pores, to get information on transport profiles of pore cross-sections. Such information with local nanoscale resolution are currently obtained using theory giving essential insights for understanding nanopore transport [22, 24, 40].

Local pH-read out is especially investigated in the context of tumor cells using dyes as molecular pH-probe [6, 41-44]. In this context, ratiometric fluorophores such as SNARF as well as the Förster resonance energy transfer (FRET) [45] dye pairs such as fluorescein isothiocyanate (FITC) and rhodamine B isothiocyanate (RITC) are commonly used [6, 41, 42, 46-49]. To date, FRET dye pairs have been combined with silica nanoparticles showing an influence of environmental conditions on the fluorescence emission allowing to use these materials as sensors [6, 42]. This approach does not allow to differentiate between dyes attached to the external or to the pore wall surface and the potential influence of spatial confinement has not been discussed. Furthermore, dye incorporation has mostly been achieved by co-condensation techniques of functionalized dyes and inorganic precursor that results in incorporation of the dyes in the metal-organic framework and only a small amount of the functionalities are chemically available [50].

Here, we report a systematic study of FRET dye pair functionalized mesoporous silica thin films (FMSFs) to understand the influence of spatial confinement on charged state of mesopores as well as the influence of the dye functionalization on pore accessibility. Therefore, the well investigated FRET dye pair FITC and RITC is immobilized in various ratios on Pluronic® F127 templated mesoporous silica thin films using post grafting. The FMSF are further analyzed with respect to their pH-dependent spectral and transport properties using UV/vis spectroscopy, fluorescence microscopy and cyclic voltammetry. Despite a possible investigation of fluorescence of FMSFs with conventional spectrometers, confocal microscopy was applied allowing future characterization with local resolution and single pore detection. To the best of our knowledge, this is the first study systematically optimizing FRET dye pair functionalization of mesopores and correlating the resulting optical monitoring of mesopore protonated states with mesopores transport characteristics which represents a first step towards localized "pH" monitoring in mesopores.

2. Experimental

2.1. Chemicals

All materials and solvents were purchased from Sigma-Aldrich, Acros Organics, and VWR and used as received unless stated otherwise. The precursor solutions for dip-coating mesoporous films were prepared using the inorganic precursor tetraethoxysilane (TEOS, Acros Organics, 98 %, Geel, Belgium) in absolute ethanol (EtOH, Merck, ≥99.5 %), with hydrochloric acid as catalyst (HCl, 37 %) and water. Pluronic® F127 (F127, BioReagent, Sigma-Aldrich, 12,600 g mol^{-1}) was used as structure directing agent at a molar ratio of 0.0075 relative to the silane precursor. Microscope slides (VWR, glass, cut edges) were cleaned in a mixture of detergent and water prior to rinsing with ethanol and drying under ambient conditions. Silicon wafers (Si-Mat, Kaufering, Germany, 100 mm diameter, 525 ± 25 µm thickness, type P/Bor, <100> orientation, CZ growth method, 2–5 W resistivity, polished on 1 side) and indium tin oxide (ITO, Delta Technologies, Ltd., Loveland, CO, USA, polished float glass, 150 x 150 x 1.1 mm, SiO_2 passivated/Indium Tin Oxide coated one surface, RS = 4–8 Ω, cut edges) were cut to desired size using a diamond cutter, cleaned using technical grade ethanol, and dried under ambient conditions prior to dip-coating of mesoporous films.

2.2. Synthesis of mesoporous thin films

Mesoporous thin films were synthesized, as described previously [10, 24, 27], via sol−gel chemistry and evaporation induced self-assembly [2] based on the silica precursor tetraethoxysilane (TEOS) in the presence of the template Pluronic® F127. The precursor solution was prepared using the following molar ratios: 1 TEOS : 40 EtOH : 0.0075 Pluronic® F127 : 10 H_2O : 0.28 HCl. The solutions were stirred for 24 h at room temperature prior to use for mesoporous film preparation. Mesoporous films were prepared on ITO coated glass, glass, or silicon wafer substrates at 40−50 % relative humidity, 25 °C, and a withdrawal speed of 2 mm/s. Freshly deposited films were stored at 40-50 % relative humidity and 25 °C in a climate chamber for 1 h. A stabilizing thermal treatment was carried out in two successive temperature steps at 60 and 130 °C for 1 h, respectively. Subsequently, the temperature was increased to 350 °C at a rate of 1 °C/min for 2 h followed by cooling down to ambient temperature, rinsing with ethanol and storage under ambient conditions. The resulting

mesoporous films are characterized by a film thickness of 150−300 nm and a porosity of ~45 vol% as measured by ellipsometry (**Table 1 and 2, ESI**).

2.3. Dye synthesis

For grafting of fluorescein isothiocyanate (FITC) and rhodamine B isothiocyanate (RITC) to the mesoporous silica, the dyes were functionalized with 3-aminopropyltrimethoxysilane (APTMS) to form N-1-(3-trimethoxysilylpropyl)-N'-fluoreceylthiourea (APTMS-FITC) and N-1-(3-trimethoxysilylpropyl)-N'-tetramethylrhodaceylthiourea (APTMS-RITC). Therefore, 6 mg (15.4 µmol, 1 eq.) FITC or 8.3 mg (15.4 µmol, 1 eq.) RITC were dissolved in 15 mL ethanol. Then, 27.63 mg ($1.54 \cdot 10^{-4}$ mol, 10 eq.) APTMS was added. The solutions were stirred for 24 h under inert conditions and used for mesoporous film functionalization without further purification.

2.4. Synthesis of FRET dye pair functionalized mesoporous silica films (FMSFs)

Dye functionalization of mesoporous silica thin films was carried out via post-grafting. A 0.01 wt% dye solution was prepared by mixing the ethanolic solution of the modified dyes with toluene under nitrogen flow followed by purging with nitrogen for 15 min. Mesoporous thin films were placed in a flask under nitrogen flow, the dye solution was added and heated to 80 °C for 1 h under inert conditions. Subsequently, the films were rinsed with toluene and ethanol to remove unbound APTMS as well as APTMS-FITC and APTMS-RITC. The dye functionalized films were stored under ambient conditions. The molar ratio of the modified dyes in the functionalization solution was varied between 1 : 1.1 : 2.2 : 1 and 10 : 1 with respect to APTMS-FITC and APTMS-RITC in the reaction solution.

2.5. pH-dependent absorption and fluorescence

For pH-dependent measurements of absorption and fluorescence emission, phosphate buffered solutions (PBS) were prepared for eight different pH values adjusted by either HCl or NaOH confirmed by using a pH electrode (pH 110, VWR). FMSFs were incubated into the pH adjusted phosphate buffered solution for 15 min and dried with pressured air directly before being measured. The stability of the applied mesoporous silica thin films in acidic (pH 2) and basic (pH 10) solution has been investigated using ellipsometry determining film thicknesses and refractive indices before and after incubation (Table S4 and S5). Fluorescence spectra were

recorded using a confocal microscope (CLSM TCS SP5 II, Leica Microsystems, Mannheim, Germany). For excitation monochromatic light of 458 nm (Ar-laser, 65 mW) was used. Fluorescence was recorded stepwise (5 nm) from 470 - 700 nm. Fluorescence images were analyzed using the Leica Application Suite AF Lite (V 2.6.3) software. Fluorescence spectra were obtained selecting three homogenous regions (250 x 250 µm) of interest (ROI) on the FMSFs. The obtained spectra were then exported to OriginPro for further processing.

UV/vis spectroscopy was performed using a Varian Cary 50 SCAN UV/vis spectrometer. The UV/vis spectra were recorded from FMSFs deposited on glass substrates in a range of 300 nm to 800 nm with a scan rate of 600 nm/min. All spectra were background corrected using an unmodified mesoporous silica film deposited on a glass substrate. UV/vis absorption spectra of CO_2-plasma treated dye functionalized mesoporous silica films are used to calculate the ratio of attached dyes according to Lambert-Beer's law. For calculations, extinction coefficients of FITC and RITC determined by Widmer et al. [42] are applied. Within all experiments the stability of the characterized silica films has been assured for the duration of the experiment e.g. using ellipsometry and cyclic voltammetry.

2.6. Attenuated Total Reflection Fourier Transform Infrared Spectroscopy (ATR-FTIR)

Infrared spectra of the prepared mesoporous films on glass or ITO substrates were performed using a Perkin Elmer Instrument One Spectrum FT-IR Spectrometer equipped with a Universal ATR Polarization Accessory (Waltham, MA, USA). All spectra were normalized to the stretching vibration of free silanol groups at ~905 cm^{-1}. The spectra were recorded using the Spectrum Software (Version 10.5.4.738, PerkinElmer, Inc. Waltham, MA, USA, 2016) between 4000 and 650 cm^{-1} with a resolution of 4 cm^{-1}, and a background as well as baseline correction was automatically performed. Additional bands of the glass substrate are visible in the FTIR spectra: Mesoporous film signals are partially superimposed by signals originating from the glass substrate in the region of 830 - 1250 cm^{-1} depending on the penetration depth of the ATR-IR evanescent waves. Nevertheless, due to the comparable film thickness, IR-spectra of different films can be compared. All further data processing was performed in OriginPro9 (ADDITIVE Soft- und Hardware für Technik und Wissenschaft GmbH, Friedrichsdorf, Germany, 2012).

2.7. Transmission Electron Microscopy (TEM)

Electron micrographs were recorded using a Philips FEI CM-20 transmission electron microscope (Philips, Amsterdam, Netherlands) equipped with a LAB-6 cathode and Olympus CCD camera, and with a maximum resolution of 2.3 Å operating at an accelerating voltage of 200 kV. Samples were prepared by scratching the mesoporous films and dispersion in filtered ethanol. After 10 min of sonication scratched mesoporous films were drop cast onto 3.05 mm Cu grids (mesh size 200) with a Lacey carbon film (Plano GmbH, article number S166-2). The samples were dried under ambient conditions.

2.8. Plasma treatment

The organic functional groups present on the exterior planar mesoporous film surface were removed by applying a CO_2-plasma treatment [28] using a Diener Femto-plasma cleaner (Diener electronic, Ebhausen, Germany) at a pressure of 0.4 mbar and power of 20 % for 12 s according to a previously published protocol by Babu et al. [51].

2.9. Cyclic voltammetry

The ionic permselectivity of the mesoporous materials was investigated via cyclic voltammetry (CV) using $[Fe(CN)_6]^{3-/4-}$ and $[Ru(NH_3)_6]^{2+/3+}$ as charged, redox-active probe molecules. Measurements were recorded using a Metrohm Autolab PGSTAT302N potentiostat. Mesoporous films prepared on ITO coated glass substrates (working electrode) were characterized using a 1 mM solution of either the positively- or negatively charged probe molecule in a PBS electrolyte solution. The pH-dependent permselectivity was investigated by adjusting the solution pH between 2 and 9 by the addition of either concentrated aqueous NaOH or HCl to the probe molecule containing buffer solutions. The pH was determined using a pH-meter (pH110, VWR). An Ag/AgCl reference electrode (BASi RE-6) and graphite counter electrode was used in the sample cell. The measured working electrode area was 0.21 cm^2. Pore accessibility for each pH was measured using a scan rate sequence of 200, 100, 25, 300, 1000, and 200 mV/s, with each scan rate being cycled three times.

3. Results and discussion

To enable monitoring of “pH” or, more precisely, protonation-/ deprotonation equilibria in functional, spatially confined mesopores, and thus enhance understanding of confinement effects as well as to get direct and ideally spatiotemporally resolved information on “pH” allowing to predict ionic transport, FRET dye pairs are a

versatile tool. To investigate their possibilities and limits, pH-sensitive FMSFs have been prepared. For the preparation and characterization of pH-sensitive FMSFs, mesoporous thin films are synthesized and subsequently functionalized with pH-reporting dyes N-1-(3-trimethoxysilylpropyl)-N'-fluoreceylthiourea (APTMS-FITC) and N-1-(3-trimethoxysilylpropyl)-N'-tetramethylrhodaceylthiourea (APTMS-RITC) by grafting them onto the mesoporous silica film pore walls (**Figure 1a**).

Allowing pH-detection of such a FRET pair within the spatial confinement of mesopores requires the fluorescence emission of one dye (here APTMS-FITC, pH-sensitive donor) to overlap with the absorption of its pair dye (here APTMS-RITC, pH-insensitive acceptor) and a FRET pair distance being small to obtain sufficient FRET and to allow detection of fluorescence emission of both dyes by exclusive irradiation of the donor dye (here APTMS-FITC). As depicted in the absorption and fluorescent emission spectra in **Figure 1b** FITC and RITC spectra sufficiently overlap. One common approach for dye-based pH-probing is the combination of one dye showing pH-sensitive photospectral properties while the second dye has to be pH-insensitive and serves as reference [52-54]. In this study, FITC represents the pH-sensitive dye while RITC serves as pH-independent reference [55-58]. Thus, for pH-monitoring both dyes have to be incorporated into the mesopores within a close distance to allow FRET to occur. Readout is performed by monitoring the fluorescence emission of both dyes after irradiation at a single wavelength of 458 nm exciting the lower wavelength absorption of FITC. In addition, the applied functionalization strategy using postgrafting of APTMS-FITC and APTMS-RITC followed by a CO_2-plasma treatment destroying dye at the external planar film surface, enables pH-monitoring FRET dye pair attachment exclusively to the mesoporous silica pore wall inside the mesopores. Alternative co-condensation would result in dyes being as well incorporated into the inorganic matrix and thus being surrounded by very different and hard to analyze local environments.

3.1. Structural and functional characterization of mesoporous thin films

The applied mesoporous silica thin films, prepared via sol-gel chemistry and EISA according to work of Brinker et al.[2], present an average film thickness of 160 nm and an ordered mesoporosity of 42 vol% as determined by ellipsometry and effective medium approximation [60] (Supporting Information and previous work [10, 23]). As demonstrated in previous work, as prepared films display organized pore arrays with pores having an ellipsoidal shape due to uniaxial contraction [23, 25] with pore connections (necks) of ~3 nm and surface area of 36 m^2 per 1 m^2 substrate surface, which corresponds to ~440 m^2/g as determined via krypton

BET adsorption [23]. According to ellipso-porosimetry analysis of previous reports [10], the pore size of mesoporous silica thin films using the same Pluronic® F127 template with identical molar ratio in the precursor formulation has been reported to be around 5.3 nm. TEM images of an unmodified mesoporous silica thin film (**Figure 1c**) show a well ordered mesoporous structure and a pore size of about 6-7 nm which is in good agreement with previous reports[23, 25] and the pore size determined in previous studies by ellipso-porosimetry[10].

Functional characterization using infrared spectroscopy shows the characteristic vibrational bands of the inorganic silica framework (**Figure 2b**). The intense vibrational mode at 905 cm^{-1} is related to free surface silanol groups. All infrared spectra are normalized to these vibrational modes of free silanol groups at 905 cm^{-1}. Vibrational modes at 1050 cm^{-1} and 1170 cm^{-1} can be assigned to the transverse and longitudinal Si-O-Si modes. In addition, transverse optical Si-O-Si vibrational modes are observed at 768 cm^{-1}. Bending vibration and stretching vibration of adsorbed water molecules are located at 1650 cm^{-1} and 3000 - 3500 cm^{-1} respectively [61]. The vibrational mode at 1595 cm^{-1}, which is overlapping with the bending vibration of water, can be assigned to the asymmetric N-H bending vibration of nitrogen containing species, particularly the thiourea group of the APTMS coupled dyes as well as remaining APTMS moieties [34] indicating successful dye functionalization. For pH-sensitive dye grafting the isothiocyanate derivates of fluorescein and rhodamine B (FITC and RITC) are modified with a silane anchor group by coupling them to 3-aminopropyltrimethoxysilane (APTMS). The resulting N-1-(3-trimethoxysilylpropyl)-N'-fluoreceylthiourea (APTMS-FITC) and N-1-(3-trimethoxysilylpropyl)-N'-tetramethylrhodaceylthiourea (APTMS-RITC) are subsequently grafted onto the silica surface (**Figure 1c**). Infrared spectroscopy of functionalized FMSFs show additional bands in comparison to the unmodified mesoporous silica thin film (**Figure 2b**): between 2800 - 3000 cm^{-1} C-H stretching bands are observed corresponding to the aromatic framework of the dyes. Furthermore, bands at 1350 - 1600 cm^{-1} can be correlated to the bending vibration of the aromatic framework of the dyes. Nevertheless, vibrational bands of the isothiocyanate group at around 2000 cm^{-1} are not present in the infrared of FMSFs indicating covalent binding of the dyes on the silica surface forming thiourea (**Figure S2, ESI**). Comparing ellipsometric measurements (**Table S1 and S2**) before and after dye functionalization reveals an increase of the refractive index of approximately 0.1 supporting the functionalization of the mesopores indicating a pore filling fraction of 68 vol% for the FMSFs with a molar ratio of 1 : 1, 1 : 2, 2 : 1 and 38 vol% for the FMSFs with a molar ratio of 10 : 1 based on effective medium calculations [10, 60]. Besides using FTIR

spectroscopy and ellipsometry dye attachment is indirectly proven by extraction experiments showing no stable attachment and successful extraction for unmodified dyes without APTMS anchor groups. In addition, FMSFs clearly show a color change visible by eye upon APTMS-RITC and APTMS-FITC binding. All together, reference experiments (**Figure S1**) together with FTIR and ellipsometry measurements as well as the color change upon APTMS-RITC and APTMS-FITC grafting, which in addition cannot be observed for planar, non-porous dense silica thin films (**Figure 2a, Figure S3**), indicate a successful attachment of APTMS-RITC and APTMS-FITC not only on the outer mesoporous silica film surface, but also to the mesopore walls representing the much larger inner surface area.

3.2. Spectral properties of FMSFs

The spectral properties of mesoporous thin films functionalized with APTMS-FITC and APTMS-RITC are investigated after grafting of different molar ratios APTMS-FITC : APTMS-RITC of 1 : 1, 1 : 2, 2 : 1 corresponding to the composition of the reaction solution resulting in grafted ratios between 1:1 to 2:1 (**Figure 2a**). Functionalized mesoporous silica films (FMSFs) are treated with CO_2-plasma [28, 51] to remove dyes attached on the outer silica surface. Spectral properties of the FMSFs are investigated via UV/vis absorption and fluorescence emission before and after CO_2-plasma treatment to compare FRET pair behavior attached exclusively on the inner mesopore wall surface with the ones attached to the planar outer surface. UV/vis absorption measurements show both absorption maxima of APTMS-FITC and APTMS-RITC at 500 nm and 560 nm (**Figure 2c, d**) proving the attachment of both dyes in the inorganic framework while retaining their spectral properties.

Comparing the absorption maximum of APTMS-FITC at 500 nm before and after CO_2-plasma treatment results in a decreasing absorption of around 15 % confirming that approximately 85 % of the dyes are attached on the inner mesopore walls, as CO_2-plasma treatment only destroys the dyes at the outer planar surface (**Figure S6**). Remarkably, most of the dyes are attached on the inner silica surface. UV/vis absorption spectra of CO_2-plasma treated dye functionalized mesoporous silica films are used to calculate the ratio of attached dyes according to Lambert-Beer's law. For calculations, extinction coefficients of FITC and RITC determined by Widmer et al. [42] are applied. The molar ratios of the dyes in the reaction solution (R1) as well as the ratios calculated from absorption spectra (R2) are compared in **Figure 2a**. The attachment of APTMS-FITC is favored compared to APTMS-RITC for all applied experimental conditions.

To investigate the pH-dependence of the spectral dye properties, the FMSFs have been immersed in phosphate buffered solutions at pH between 2 and 9 for 15 minutes. An absorption color change of the dye functionalized silica films can be observed after incubation in different pH solutions as depicted in **Figure 2a**. The spectral properties of fluorescein have been widely studied in the past. In aqueous solution fluorescein exists in four different prototropic forms depending on the solution pH [56, 58]. These can be directly differentiated by pH-dependent UV/vis absorption studies of FITC in phosphate buffered solution (**Figure 2c**) as described in the literature[62]. In solution the pH-dependent UV/vis spectra of FITC shown in **Figure 2c** all expected forms, the cationic form at pH 2 (black spectrum), the zwitterionic chinoid or lactone form at pH 3 (red spectrum), the monoanionic form at pH 5 (magenta spectrum) and the dianionic form at pH 7 (marine spectrum), are observed. In contrast to the absorption spectra of FITC in solution, the absorption spectra of APTMS-FITC grafted to the CO_2-plasma treated mesoporous silica films do not show all prototropic forms (**Figure 2d**). In the presence of buffer solution at pH 2, the cationic form cannot be observed. This probably indicates an influence of the mesopore's spatial confinement and a proton transfer between FITC and amine groups of unfunctionalized APTMS. Unfortunately, a determination of the relative amount of different prototropic forms is not possible due to overlapping absorption spectra. In addition, the absorption of APTMS-RITC reference dye at 560 nm does not change with pH (**Figure S4**). This allows to use the absorption maximum of APTMS-RITC as reference. All absorption spectra are normalized to the APTMS-RITC absorption maximum at 560 nm. Comparing the evolution of the absorption maxima of FITC or APTMS-FITC at 485 - 500 nm an increase of the relative absorption of FITC in solution as well as of APTMS-FITC bound to the mesoporous silica film with increasing solution pH is observed. Furthermore, the pH-induced change of the relative FITC absorption shows a comparable behavior for FITC in solution and APTMS-FITC bound to the mesoporous silica film (**Figure 2e)**. Varying solution pH from pH 2 to pH 9 results in an almost linear increase by a factor of three of APTMS-FITC absorption at 485 - 500 nm relative to the APTMS-RITC absorption at 560 nm for FMSFs showing the maintained pH-sensing properties of the FRET pair after covalent attachment. Comparing the pH-dependent absorption maxima of APTMS-FITC at 485 - 500 nm for FMSFs with different molar ratios of APTMS-FITC : APTMS-RITC before and after CO_2-plasma treatment (**Figure 2f**), an overall decrease of the absorption intensity and a reduced change of APTMS-FITC absorption with pH is observed after destroying the dyes at the outer planar surface. This reduced relative APTMS-FITC absorption change with pH for dyes located inside the mesopores indicates a lower "pH" in the mesopores probably due to a confinement effect on local pH

assuming no reduced APTMS-FITC : APTMS-RITC ratio inside the pores as compared to the outer planar surface. In any case, a pH-sensitive regime of up to six pH units for these mesopores is observed (**Figure 2**).

Besides absorption, fluorescence emission based pH-detection using FRET in mesoporous thin films allows a ratiometric pH-detection inside mesopores. Fluorescence spectra are obtained using a confocal microscope, measuring three homogenous regions of interest (ROI) on a FMSFs as depicted in **Figure 3a**. Readout by confocal microscopy bares the future potential for local resolution and single pore detection. The fluorescence spectra of FMSFs show an emission maximum at 520 nm which can be attributed to APTMS-FITC as well as an emission maximum at 585 nm, attributed to APTMS-RITC (**Figure 3b**). Since the excitation wavelength at 458 nm only overlaps with absorption of APTMS-FITC (donor), the observed APTMS-RITC (acceptor) fluorescence emission proofs the expected energy transfer from APTMS-FITC as the donor to APTMS-RITC as the acceptor. Additionally, the maximum fluorescence intensity of APTMS-RITC (585 nm) is significantly higher than the maximum fluorescence intensity of APTMS-FITC (520 nm) indicating an efficient energy transfer (**Figure S12**). Consequently, both dyes, APTMS-FITC and APTMS-RITC, must be located close to each other within the mesopores. All fluorescence spectra recorded after immersion in buffer solution of pH 2 to pH 9 are normalized to the emission maximum of RITC at 585 nm followed by monitoring the pH-dependent evolution of the maximum emission of FITC at 520 nm. With increasing solution pH from pH 2 to pH 9 an increasing fluorescence emission of the donor dye APTMS-FITC is observed showing a linear dependence of relative fluorescence intensity on pH as depicted in **Figure 3c**. Interestingly, the pH-dependent regime is extended from two to three pH units upon changing the molar APTMS-FITC : APTMS-RITC ratio within the reaction solution from 1 : 1 to 1 : 2 (**Figure 3c**). This is as well observed after CO_2-plasma treatment, indicating that the APTMS-FITC : APTMS-RITC concentration strongly determines the detectable pH-range, and that an excess of APTMS-FITC is necessary to allow FRET to occur while simultaneously detecting a broad pH-range. Comparing the fluorescence emission intensity before and after the CO_2-plasma treatment, a decrease of the overall fluorescence intensities is observed, in analogy to the observations made for the UV/vis absorption proving removal of dye from the outer planar FMSFs surface, as discussed above. After CO_2-plasma treatment a reduced change in fluorescence emission intensity upon pH-screening, in accordance with UV-vis absorption, is observed. This either indicates a higher amount of attached APTMS-FITC than of attached APTMS-RITC on the outer FMSFs surface than on the inner surface or a lower pH in the mesopores indicating a confinement effect on local pH. Overall, the fluorescence intensity of the emission maximum of APTMS-FITC at 520 nm is

relatively small compared to the emission maximum of APTMS-RITC at 585 nm due to an efficient energy transfer, which limits experimental pH resolution as the donor dye is used for pH-detection. An enhanced resolution in fluorescence based pH detection is obtained improving FMSF's functionalization by using a molar ratio of APTMS-FITC : APTMS-RITC = 10 : 1 resulting in a grafted APTMS-FITC : APTMS-RITC ratio of 3 : 1 (**Figure S7**). The fluorescence emission intensity of this functionalized FMSFs show a broad linear range of pH-dependent changes from pH 4 to pH 9 in fluorescence emission after CO_2-plasma (**Figure 3d**). Additionally, an enhanced slope of pH-dependent relative maximum fluorescence emission intensity of APTMS-FITC is observed as compared to the FMSFs generated with APTMS-FITC : APTMS-RITC reaction solution ratios of 1 : 1 , 1 : 2 and 2 : 1 resulting in a more precise determination of pH. Consequently, a higher ratio of APTMS-FITC to APTMS-RITC, achieved by increasing the APTMS-FITC ratio within the reaction solution, leads to an improved detection based on the fluorescence intensity monitoring the emission maximum of APTMS-FITC at 520 nm and the pH-detection range can be tuned varying the grafted APTMS-FITC to APTMS-RITC ratio.

In conclusion, FRET dye pair functionalization of mesoporous thin films can be used for pH-detection observing the absorption or fluorescence emission if the FRET pair consists of a pH-sensitive dye combined with a pH-insensitive reference dye both covalently grafted to the mesopore wall. Thereby, the range of pH detection by monitoring the fluorescence emission is comparable to similar mesoporous silica nanoparticles[6], but the range of pH detection is extended to a broad range from pH 2 to pH 8 by observing the absorption of the FRET pair. An optimized detection with respect to magnitude of signal and relative ratio needs an optimization of the covalently attached dye ratio as well as consideration of preferred binding due to pore wall–dye interaction, molecular size, and competition with respect to pore accessibility and reaction with other molecules present in solution. Optimized detection is achieved by tuning the APTMS-FITC (donor, pH-sensitive) to APTMS-RITC (acceptor, reference dye) ratio such that only few APTMS-FITC (donor) molecules couple to APTMS-RITC (acceptor, reference) molecules to allow ratiometric detection but at the same time not to lose too much pH-sensitivity by FRET. In summary, 85 % of the attached dyes are located within the mesopores (**Figure S6**) probing "pH" in this confined space. Based on their absorption and fluorescence emission a linear detection regime of up to six pH units has been implemented after optimization of the functionalization procedure. Furthermore, comparing absorption and fluorescence with and without dyes present at the outer planar mesoporous film surface, the influence of the spatial mesopore confinement on "pH"

can be observed. Finally, for these experiments only a single excitation wavelength is required and by using high resolution fluorescence microscopy techniques local information and single pore measurements are possible.

3.3. Correlation to ionic permselectivity of mesoporous thin films

The monitoring of protonation–deprotonation equilibria in mesopores is especially relevant to predict and design mesopore accessibility and transport. To the best of our knowledge, transport properties haven't been experimentally correlated with dye-based pH-sensing in mesoporous materials. To investigate the ionic transport properties of FMSFs, the diffusion of charged probe molecules through mesoporous films supported on ITO substrates is investigated using cyclic voltammetry (CV), monitoring anionic and cationic electroactive redox probes $[Fe(CN)_6]^{3-/4-}$ and $[Ru(NH_3)_6]^{2+/3+}$, respectively. The observed pH-dependent mesopore accessibility is correlated to FRET dye pair based pH-detection (**Figure 4, 5**). Due to the presence of unreacted silanol groups, amino groups, and covalently attached APTMS-RITC and APTMS-FITC on the silica pore wall, a pH-dependent charge of the pore wall, and thus an ionic permselectivity of the mesoporous film is expected. In general, ionic permselectivity has been demonstrated for a variety of functionalized nanopores [1, 32, 33] and is mostly discussed with respect to gating of mesopore accessibility. Here, under acidic conditions, protonated amino groups are expected to result in a positively charged mesopore wall whereas basic conditions should result into deprotonated remaining silanol groups, deprotonated fluorescein, and deprotonated rhodamine B molecules, and thus a negatively charged mesopore. As the mesopore diameter is in the range of the Debye screening length, equally charged ions should be electrostatically excluded and countercharged ions should access the pore or even be preconcentrated inside the mesopores. Redox probe molecules are oxidized and reduced below the mesoporous film at an ITO electrode and thus result in a current in the cyclic voltammogram. Cyclic voltammograms of a FMSF and unmodified mesoporous silica thin film recorded at different solution pH values are shown in **Figure 4a** and **4b**. As expected, the cyclic voltammograms of FMSFs show accessibility of negatively charged probe molecules under acidic conditions, whereas electrostatic exclusion of these negatively charged probe molecules is observed under basic conditions. The resulting pH-dependent peak current density is shown in **Figure 4b, d**. Thereby, the enhanced peak current densities of the FMSF as compared to unmodified mesoporous silica and the broadened electrochemical response indicate a preconcentration of the negatively charged probe molecule $[Fe(CN)_6]^{3-/4-}$ within the functionalized

mesoporous framework due to attractive electrostatic interaction. At pH values above pH 5, deprotonation of remaining silanol groups as well as APTMS-FITC molecules at the pore wall leads to an electrostatic repulsion of negatively charged molecules resulting in a pH-dependent decrease of peak current density down to electrostatic exclusion. Simultaneously, accessibility and preconcentration of the positively charged probe molecules are observed under these basic conditions, while an electrostatic exclusion of the positively charged probe molecule $[Ru(NH_3)_6]^{2+/3+}$ occurs in acidic environment. The peak current densities in dependence of pH result in titration curves with a sigmoidal shape (**Figure 4b**). The inflection point of these curves at a pH value of 5.8 corresponds to the pK_a value which in case of mesoporous films should reflect the pK_a of the functionalized mesopores. The pK_a value of 5.8 is close to the monoanion/dianion transition of fluorescein reported in literature [57, 58]. Comparing this pK_a value with the value obtained from titration of FITC with protons in buffer solution using the emission intensity at 515 nm (**Figure S11**) a shift from pK_a 6.3 to 5.8 is observed. This shift of 0.5 pH units indicates the influence of the mesopore environment.

Comparing the maximum peak current density obtained from FMSFs to unmodified mesoporous silica thin films, a higher maximum peak current density is observed for FMSFs at acidic pH, whereas a lower maximum peak current density is observed for $[Fe(CN)_6]^{3-/4-}$ at basic pH. Consequently, the influence of remaining silanol groups seems to be less important for the observed transport properties of FMSFs than the free amine groups and dyes which is in accordance to the obtained pore filling after functionalization. Consistently, at pH > 5 higher $[Ru(NH_3)_6]^{2+/3+}$ peak current densities for the unmodified mesoporous silica thin film than for the FMSF are observed due to the electrostatic attraction and preconcentration of probe molecules in the negatively charged mesoporous silica film. Overall, the behavior of both probe molecules indicates, in accordance to dye-based monitoring discussed above, that the surface charge of FMSFs is dominated by the positively charged amino groups present on the wall surface at pH < 5 and remaining silanolate groups as well as deprotonated fluorescein and rhodamine B moieties at basic pH. Nevertheless, FMSFs show high ion permselectivity which can be tuned by varying pH as expected. This clearly shows that FRET dye pair functionalization is a suitable tool for “pH”-readout in mesopores, investigation of confinement effects, and its correlation to mesopores accessibility and allows application of FMSFs as sensors and membranes with gate like properties. But for pH-readout and especially when it comes to local resolution, the influence of the dyes itself on the transport properties has to be considered as well. In this regard, a minimal functional density might be recommended as well supporting high resolution microscopy techniques for readout.

Combining the detected mesopore accessibility with FRET dye pair based pH readout shows that both pH-detection results based on absorption and ratiometric FRET fluorescence emission match the observed mesopore transport characteristics (**Figure 5**). Furthermore, the confinement specific shifted pK_a value is reproduced supporting spatial influence on pore accessibility (CO_2-plasma treated films). This confirms the applicability of the installed in-situ pH-readout system based on APTMS-RITC and APTMS-FITC in silica mesopores, it represents a first step towards quantitative analysis of these shifts, and underlines the importance of knowing protonation-deprotonation equilibria and charge density of mesopores to understand their transport properties. Together with the possibility of using high resolution (confocal) microscopy techniques, single pore analysis is envisioned going beyond classical averaging information on surface pH. But it has to be noted as well, that the FRET dye pair not only serves for pH-readout but, in the applied concentration, clearly influences mesopore characteristics such as ionic permselectivity. However, molecular pH-readout based on FRET-pair absorption and fluorescence emission correlates well with the observed ionic permselectivity and thus represents optical means to detect charge state of mesopores and to optically detect transport of nanoporous materials.

Conclusions

With this study we provide a systematic strategy to optimally combine mesoporous silica films with a pH-sensitive FRET dye pair allowing to exclusively functionalize the mesopore wall after destroying the dyes at the external planar film surface. Thereby, approximately 85 % of the dyes are located at the mesopore walls and not on the outer mesoporous film surface. Systematic variation of APTMS-RITC : APTMS-FITC ratio in the reaction solution and analysis of resulting absorption spectra indicate that grafting of APTMS-FITC is favored compared to grafting of APTMS-RITC. After optimization of dye grafting and destroying the dyes on the external mesoporous film surface, a pH-dependent linear detection regime of up to six pH units is obtained monitoring absorption or fluorescence emission of FMSFs. Thereby, the optimized pH detection range of six pH units is obtained for FMSFs prepared with a APTMS-FITC : APTMS-RITC ratio of 10 : 1 in the reaction solution resulting in a grafted ratio of 3 : 1 indicating an optimized pH detection with an access of APTMS-FITC (pH-sensitive, FRET donor). The detected “pH” by FRET dye pair absorption or fluorescence emission correlates well with the pH-dependent ionic permselectivity detected by cyclic voltammetry as well reproducing the expected confinement-based pK_a shift of mesopores as compared to solution pKa. This confirms the

importance of monitoring protonation-deprotonation equilibria and charge density of mesopores to understand their transport properties especially for complex functional pores such as responsive or gradient-functionalized mesopores. In addition, this study shows the versatility of FRET dye pairs consisting of a pH-sensitive dye and a pH-insensitive reference dye to monitor protonation-deprotonation equilibria in spatially confined nanopores but as well emphasizes the need for optimization of functional density of FRET dye pairs, e.g. to reduce the influence of the dye probe molecules on the mesopores characteristics itself. For further investigation of pH differences in mesopores with respect to bulk solution, and direct monitoring of pH even in single pores, low functional dye densities and ratiometric dyes are envisioned, and are currently under investigation.

Acknowledgements

We kindly acknowledge the financial support by the LOEWE Research Cluster "iNAPO" of the Hessen State Ministry of Higher Education, Research and the Arts. Mrs. Kunz and Prof. Dr. Achim Kleebe (TU-Darmstadt) are acknowledged for their support with TEM measurements. We also thank Prof. Dr. Wolfgang Ensinger for providing access to profilometer measurements in the department of material science (TU Darmstadt).

References

1. Walcarius, A., *Mesoporous materials and electrochemistry.* Chem. Soc. Rev., 2013. **42**(9): p. 4098-140.
2. Brinker, C.J., et al., *Evaporation-induced self-assembly: Nanostructures made easy.* Adv. Mater., 1999. **11**(7): p. 579-585.
3. Shenderovich, I.G., et al., *Pyridine-15N A Mobile NMR Sensor for Surface Acidity and Surface Defects of Mesoporous Silica.* J. Phys. Chem. B, 2003. **107**(43): p. 11924-11939.
4. Pal, N. and A. Bhaumik, *Soft templating strategies for the synthesis of mesoporous materials: Inorganic, organic–inorganic hybrid and purely organic solids.* Adv. Colloid Interface Sci., 2013. **189-190**(Supplement C): p. 21-41.
5. Salonen, J., et al., *Mesoporous silicon microparticles for oral drug delivery: loading and release of five model drugs.* J. Control. Release, 2005. **108**(2-3): p. 362-74.
6. Lei, J., L. Wang, and J. Zhang, *Ratiometric pH sensor based on mesoporous silica nanoparticles and Forster resonance energy transfer.* Chem. Commun. (Camb), 2010. **46**(44): p. 8445-8447.
7. Malfatti, L., et al., *Nanocomposite mesoporous ordered films for lab-on-chip intrinsic surface enhanced Raman scattering detection.* Nanoscale, 2011. **3**(9): p. 3760-6.
8. Vaseashta, A. and D. Dimova-Malinovska, *Nanostructured and nanoscale devices, sensors and detectors.* Sci. and Technol. Adv. Mater., 2005. **6**(3-4): p. 312-318.

9. Sun, M.H., et al., *Applications of hierarchically structured porous materials from energy storage and conversion, catalysis, photocatalysis, adsorption, separation, and sensing to biomedicine.* Chem. Soc. Rev., 2016. **45**(12): p. 3479-563.
10. Brunsen, A., et al., *Manipulation of molecular transport into mesoporous silica thin films by the infiltration of polyelectrolytes.* Langmuir, 2011. **27**(8): p. 4328-4333.
11. Unger, K.K., et al., *Liquid Chromatography-Its Development and Key Role in Life Science Applications.* Angew. Chem. Int. Ed., 2010. **49**(13): p. 2300-2312.
12. Unger, K.K. and A.I. Liapis, *Adsorbents and columns in analytical high-performance liquid chromatography: A perspective with regard to development and understanding.* J. Sep. Sci., 2012. **35**: p. 1201-1212.
13. Giménez, C., et al., *Towards Chemical Communication between Gated Nanoparticles.* Angew. Chem. Int. Ed., 2014. **53**: p. 12629-12633.
14. Benezra, M., et al., *Multimodal silica nanoparticles are effective cancer-targeted probes in a model of human melanoma.* J. Clin. Investig., 2011. **121**: p. 2768-2780.
15. Murison, J., et al., *Wetting Heterogeneities in Porous Media Control Flow Dissipation.* Phys. Rev. Appl., 2014. **2**: p. 034002.
16. Fan, R., et al., *Gated proton transport in aligned mesoporous silica films.* Nat. Mater., 2008. **7**(4): p. 303-7.
17. Feng, L., et al., *A super-hydrophobic and super-oleophilic coating mesh film for the separation of oil and water.* Angew. Chem. Int. Ed. Engl, 2004. **43**(15): p. 2012-4.
18. Kwon, G., et al., *On-demand separation of oil-water mixtures.* Adv. Mater., 2012. **24**(27): p. 3666-71.
19. Leung, K., I.M.B. Nielsen, and L.J. Criscenti, *Elucidating the Bimodal Acid-Base Behavior of the Water-Silica Interface from First Principles* J. Am. Chem. Soc., 2009. **131**: p. 18358-18365.
20. Hair, M.L. and W. Hertl, *Acidity of Surface Hydroxyl Groups.* J. Phys. Chem. , 1970. **74**: p. 91-94.
21. Rosenholm, J.M., et al., *On the Nature of the Brønsted Acidic Groups on Native and Functionalized Mesoporous Siliceous SBA-15 as Studied by Benzylamine Adsorption from Solution.* Langmuir, 2007. **23**: p. 4315-4323.
22. Tagliazucchi, M., O. Azzaroni, and I. Szleifer, *Responsive Polymers End-Tethered in Solid-State Nanochannels: When Nanoconfinement Really Matters.* J. Am. Chem. Soc., 2010. **132**: p. 12404–12411.
23. Silies, L., et al., *Mesoporous Thin Films, Zwitterionic Monomers, and Iniferter-Initiated Polymerization: Polymerization in a Confined Space.* Chem. Mater., 2015. **27**(6): p. 1971-1981.
24. Andrieu-Brunsen, A., et al., *Mesoporous Hybrid Thin Film Membranes with PMETAC@Silica Architectures: Controlling Ionic Gating through the Tuning of Polyelectrolyte Density.* Chem. Mater., 2015. **27**(3): p. 808-821.
25. Tom, J., et al., *Optimisation of Surface-Initiated Photoiniferter-Mediated Polymerisation under Confinement, and the Formation of Block Copolymers in Mesoporous Films.* Polymers, 2017. **9**(10): p. 539.
26. Banghart, M.R., et al., *Photochromic blockers of voltage-gated potassium channels.* Angew. Chem. Int. Ed. Engl, 2009. **48**(48): p. 9097-101.
27. Brunsen, A., et al., *Proton and calcium-gated ionic mesochannels: phosphate-bearing polymer brushes hosted in mesoporous thin films as biomimetic interfacial architectures.* Langmuir, 2012. **28**(7): p. 3583-92.

28. Krohm, F., et al., *Photochromic spiropyran- and spirooxazine-homopolymers in mesoporous thin films by surface initiated ROMP.* J. Mater. Chem. C, 2016. **4**(18): p. 4067-4076.
29. Wang, G., et al., *Photon Gated Transport at the Glass Nanopore Electrode.* J. Am. Chem. Soc., 2006. **128**: p. 13553-13558.
30. Xiao, K., L. Wen, and L. Jiang, *Biomimetic Solid-State Nanochannels: From Fundamental Research to Practical Applications.* Small, 2016. **12**: p. 2810-2813.
31. Xiao, K., et al., *Construction and application of photoresponsive smart nanochannels.* J. Photochem. Photobiol. C: Photochem. Rev., 2016. **26**: p. 31-47.
32. Alberti, S., G.J.A.A. Soler-Illia, and O. Azzaroni, *Gated supramolecular chemistry in hybrid mesoporous silica nanoarchitectures: controlled delivery and molecular transport in response to chemical, physical and biological stimuli.* Chem. Commun., 2015. **51**: p. 6050-6075.
33. Soler-Illia, G.J.A.A. and O. Azzaroni, *Multifunctional hybrids by combining ordered mesoporous materials and macromolecular building blocks.* Chem. Soc. Rev., 2011. **40**(2): p. 1107-1150.
34. Calvo, A., et al., *Mesoporous aminopropyl-functionalized hybrid thin films with modulable surface and environment-responsive behavior.* Chem. Mater., 2008. **20**(14): p. 4661-4668.
35. Silies, L. and A. Andrieu-Brunsen, *Programming Ionic Pore Accessibility in Zwitterionic Polymer Modified Nanopores.* Langmuir, 2017.
36. Gilles, F.M., et al., *Ionic Conductance of Polyelectrolyte-Modified Nanochannels: Nanoconfinement Effects on the Coupled Protonation Equilibria of Polyprotic Brushes.* J. Phys. Chem. C, 2016. **120**(9): p. 4789-4798.
37. Longo, G.S., M.O. de la Cruz, and I. Szleifer, *Molecular theory of weak polyelectrolyte thin films.* Soft Matter, 2012. **8**(5): p. 1344-1354.
38. Longo, G.S., M. Olvera de la Cruz, and I. Szleifer, *Molecular Theory of Weak Polyelectrolyte Gels: The Role of pH and Salt Concentration.* Macromolecules, 2011. **44**: p. 147-158.
39. Wang, D., et al., *How and Why Nanoparticle's Curvature Regulates the Apparent pK(a) of the Coating Ligands.* J. Am. Chem. Soc., 2011. **133**(7): p. 2192-2197.
40. Silies, L., et al., *Insights into the Role of Counterions on Polyelectrolyte-Modified Nanopore Accessibility.* Langmuir, 2018. **34**(20): p. 5943-5953.
41. Peng, H.S., et al., *A nanogel for ratiometric fluorescent sensing of intracellular pH values.* Angew. Chem. Int. Ed. Engl, 2010. **49**(25): p. 4246-9.
42. Widmer, S., et al., *Incorporation of a FRET dye pair into mesoporous materials: a comparison of fluorescence spectra, FRET activity and dye accessibility.* Analyst, 2015. **140**(15): p. 5324-34.
43. Chiappini, C., et al., *Mapping Local Cytosolic Enzymatic Activity in Human Esophageal Mucosa with Porous Silicon Nanoneedles.* Adv. Mater., 2015. **27**(35): p. 5147-52.
44. Chiappini, C., et al., *Biodegradable Nanoneedles for Localized Delivery of Nanoparticles in Vivo: Exploring the Biointerface.* ACS Nano, 2015. **9**(5): p. 5500-5509.
45. Förster, T., *Zwischenmolekulare Energiewanderung und Fluoreszenz.* Ann. Phys., 1948. **437**(1-2): p. 55-75.
46. Bottenus, D., et al., *Experimentally and theoretically observed native pH shifts in a nanochannel array.* Lab Chip, 2009. **9**(2): p. 219-31.
47. Thörn, C., et al., *A method to measure pH inside mesoporous particles using protein-bound SNARF1 fluorescent probe.* Microporous Mesoporous Mater., 2013. **165**: p. 240-246.
48. Zhu, S., W. Lin, and L. Yuan, *Development of a ratiometric fluorescent pH probe for cell imaging based on a coumarin–quinoline platform.* Dyes Pigment., 2013. **99**(2): p. 465-471.

49. Chen, Y.-P., et al., *Surface charge effect in intracellular localization of mesoporous silicananoparticles as probed by fluorescent ratiometric pH imaging.* RSC Adv., 2012. **2**(3): p. 968-973.
50. Calvo, A., et al., *Chemical reactivity of amino-functionalized mesoporous silica thin films obtained by co-condensation and post-grafting routes.* Microporous Mesoporous Mater., 2009. **121**(1-3): p. 67-72.
51. Babu, D.J., et al., *Carbon Dioxide Plasma as a Versatile Medium for Purification and Functionalization of Vertically Aligned Carbon Nanotubes.* J. Phys. Chem. C, 2014. **118**(22): p. 12028-12034.
52. Dey, D., et al., *Development of an ion-sensor using fluorescence resonance energy transfer.* Sens Actuator B: Chem, 2014. **195**: p. 382-388.
53. Burns, A., H. Ow, and U. Wiesner, *Fluorescent core-shell silica nanoparticles: towards "Lab on a Particle" architectures for nanobiotechnology.* Chem. Soc. Rev., 2006. **35**(11): p. 1028-42.
54. Peng, J., et al., *Noninvasive monitoring of intracellular pH change induced by drug stimulation using silica nanoparticle sensors.* Anal. Bioanal. Chem., 2007. **388**(3): p. 645-54.
55. Tsou, C.-J., Y. Hung, and C.-Y. Mou, *Hollow mesoporous silica nanoparticles with tunable shell thickness and pore size distribution for application as broad-ranging pH nanosensor.* Microporous Mesoporous Mater., 2014. **190**: p. 181-188.
56. Martin, M.M. and L. Lindqvist, *THE pH DEPENDENCE OF FLUORESCEIN FLUORESCENCE.* J. Lumin., 1975. **10**: p. 381-390.
57. Klonis, N., et al., *Spectral properties of fluorescein in solvent-water mixtures: Applications as a probe of hydrogen bonding environments in biological systems.* J. Photochem. Photobiol., 1998. **67**(5): p. 500-510.
58. Sjoback, R., J. Nygren, and M. Kubista, *Absorption and Fluorescence Properties of Fluorescein.* Spectrochim. Acta A, 1995. **51**(6): p. L7-L21.
59. Stryer, L., *FLUORESCENCE ENERGY TRANSFER AS A SPECTROSCOPIC RULER.* Ann. Rev. Biochem, 1978. **47**: p. 819-846.
60. Boissiere, C., et al., *Porosity and mechanical properties of mesoporous thin films assessed by environmental ellipsometric porosimetry.* Langmuir, 2005. **21**(26): p. 12362-71.
61. Innocenzi, P., *Infrared spectroscopy of sol-gel derived silica-based films: a spectra-microstructure overview.* J. Non-Cryst. Solids, 2003. **316**(2-3): p. 309-319.
62. Klonis, N. and W.H. Sawyer, *Spectral properties of the prototropic forms of fluorescein in aqueous solution.* J. Fluoresc., 1996. **6**(3): p. 147-57.

Figure captions

Figure 1. a) Scheme showing the FRET dye pair (FITC, green, donor and RITC, orange, acceptor) functionalized mesoporous silica film (FMSF). **b)** Molecular structure as well as absorption (solid line) and fluorescence emission (dashed line) spectra of FITC (green) and RITC (orange) recorded in ethanol. **c)** Representative TEM image of a mesoporous silica thin film, scale bar: 50 nm (left) and 100 nm (right).

Figure 2. a) Image of FMSF deposited on glass substrates in dependence of incubation solution pH between pH 2 and pH 9. R1: Ratio of APTMS-FITC : APTMS-RITC in the reaction solution, R2: calculated ratio of FITC : RITC on FMSFs. **b)** ATR-FTIR spectra of a FMSF with a APTMS-FITC : APTMS-RITC molar ratio of 10 : 1 in the reaction solution (red) in comparison to a bare mesoporous silica film (black). Both spectra are normalized to the stretching vibration of free silanol groups at 905 cm^{-1}. **c)** Absorption spectra of FITC : RITC = 2 : 1 in PBS buffer solution with varying pH. Absorption spectra are normalized to the absorption maxima of RITC at 560 nm. **d)** Absorption spectra of FMSF with a molar ratio of 2 : 1 with respect to APTMS-FITC and APTMS-RITC in the reaction solution in dependence of pH after CO_2-plasma treatment. Absorption spectra are normalized to the absorption maxima of RITC at 560 nm. **e)** Absorption maxima at 485 - 500 nm of FITC in dependence of pH of a FMSF with the molar ratio 2 : 1 (red) and in solution with a molar ratio of 2 : 1 (black). **f)** pH-dependent absorption maxima of FITC in FMSFs for molar ratios 1 : 1 (black), 1 : 2 (red) and 2 : 1 (blue) with respect to APTMS-FITC and APTMS-RITC in the reaction solution before (spheres, dashed line) and after CO_2-plasma treatment (circles, solid line). The CO_2 plasma treatment destroys attached dyes at the external planar mesoporous film surface. The absorption is recorded at a wavelength of 485 - 500 nm. Lines represent linear fits.

Figure 3. a) Representative pseudocolor image (775 x 775 μm) from CLSM of a FMSF shown in a "glow over/ glow under" lookup table with three chosen ROIs on homogeneous spots of the film. **b)** Fluorescence spectra of a FMSF after CO_2-plasma treatment with an APTMS-FITC : APTMS-RITC molar ratio of 10 : 1 in the reaction solution. Spectra are normalized to the emission maxima of APTMS-RITC at 585 nm. **c)** Linear dependence of fluorescence emission intensity on pH for FMSFs with APTMS-FITC : APTMS-RITC molar ratios of 1 : 1 (black), 1 : 2 (red) and 2 : 1 (blue) in the reaction solution before (spheres, dashed line) and after CO_2-plasma treatment (circles, solid line). The ratio between the fluorescence intensities of FITC at 520 nm and RITC at 585 nm is plotted in dependence of pH. **d)** Linear dependence of fluorescence emission intensity on pH detected using FMSFs functionalized with APTMS-FITC : APTMS-RITC molar ratios of 1 : 1 (black), 1 : 2 (red), 2 : 1 (blue) and 10 : 1 (green) in the reaction solution.

Figure 4. a) Cyclic voltammograms (scan rate 100 mV/s) recorded in PBS buffer solution as supporting electrolyte at pH 2 - 10 using the redox active probe molecules $[Fe(CN)_6]^{3-/4-}$ (1 mM) and $[Ru(NH_3)_6]^{2+/3+}$

(1 mM) for a FMSF functionalized in presence of a APTMS-FITC : APTMS-RITC molar ratio of 10 : 1 in the reaction solution and **b)** its pH-dependent maximum current density of $[Fe(CN)_6]^{3-/4-}$ and $[Ru(NH_3)_6]^{2+/3+}$ reflecting mesopore accessibility. **c)** Cyclic voltammograms (scan rate 100 mV/s) recorded in PBS buffer solution as supporting electrolyte at pH 2 - 10 using the redox active probe molecules $[Fe(CN)_6]^{3-/4-}$ (1 mM) and $[Ru(NH_3)_6]^{2+/3+}$ (1 mM) for an unmodified mesoporous silica thin film and **d)** its maximum current density of $[Fe(CN)_6]^{3-/4-}$ and $[Ru(NH_3)_6]^{2+/3+}$ in dependence of pH reflecting mesopore accessibility. The lines in b) and c) represent sigmoidal fits.

Figure 5. pH-dependent maximum current density of the probe molecule $[Ru(NH_3)_6]^{3-/4-}$ (black spheres, sigmoidal fit) as well as pH-dependent fluorescence emission intensity (red spheres) and pH-dependent absorption maxima of FITC (blue spheres) for FMSF functionalized with a APTMS-FITC : APTMS-RITC molar ratio of 10 : 1 in the reaction solution.

Figures

Figure 1

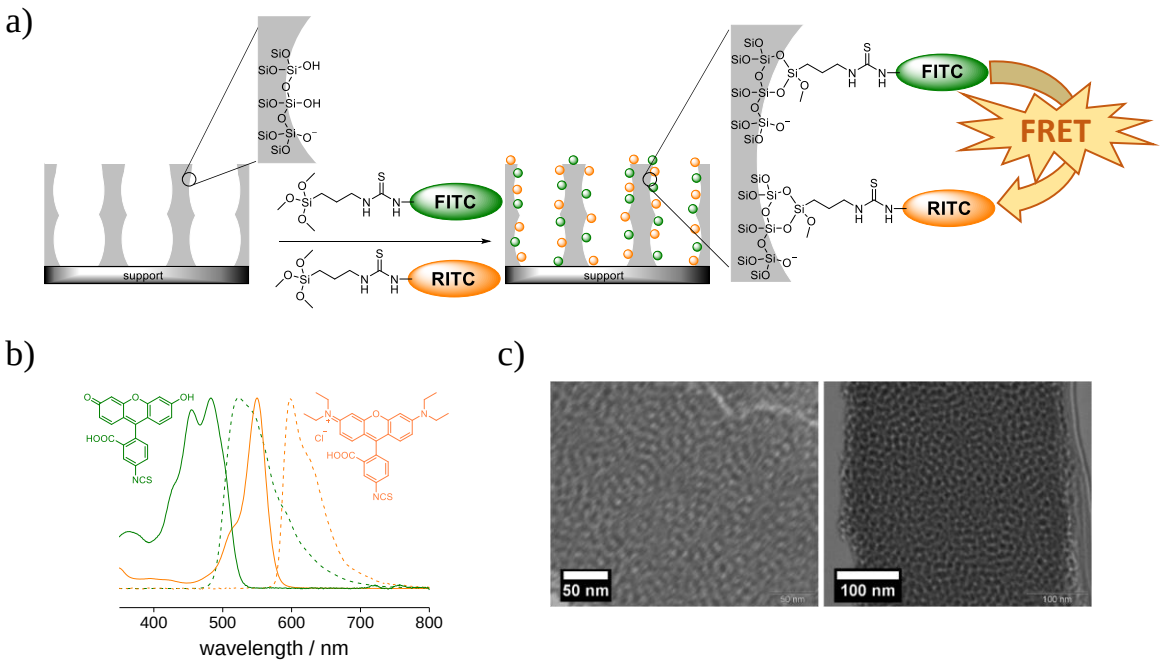

Figure 2

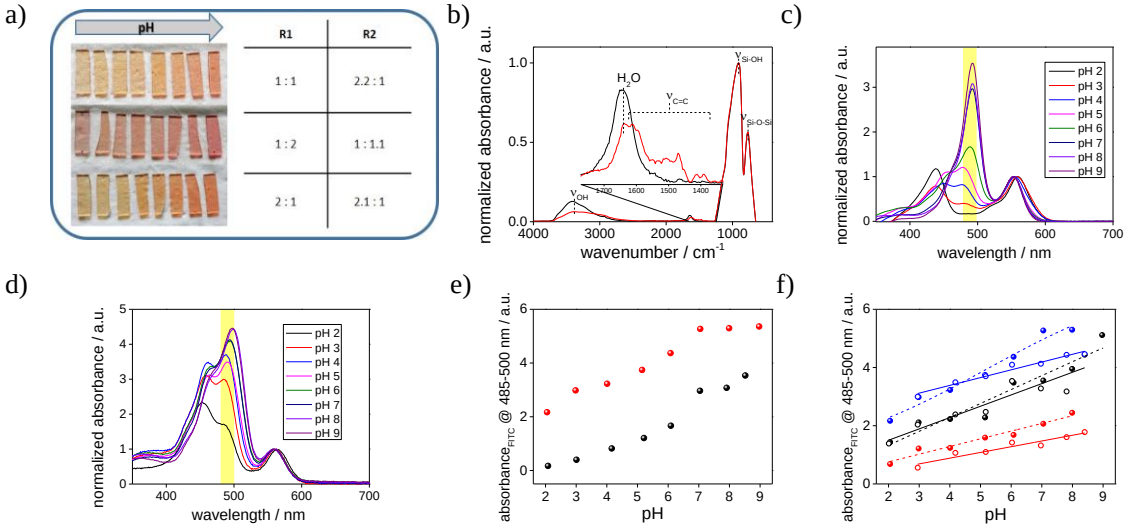

Figure 3

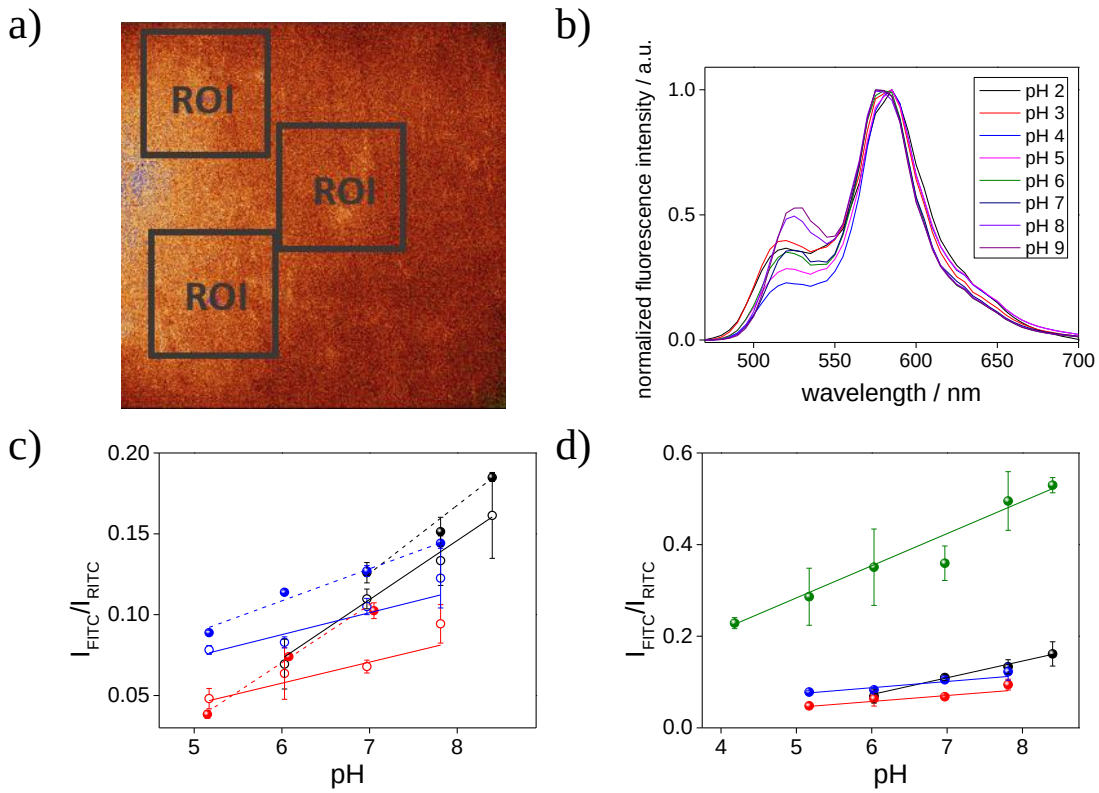

Figure 4

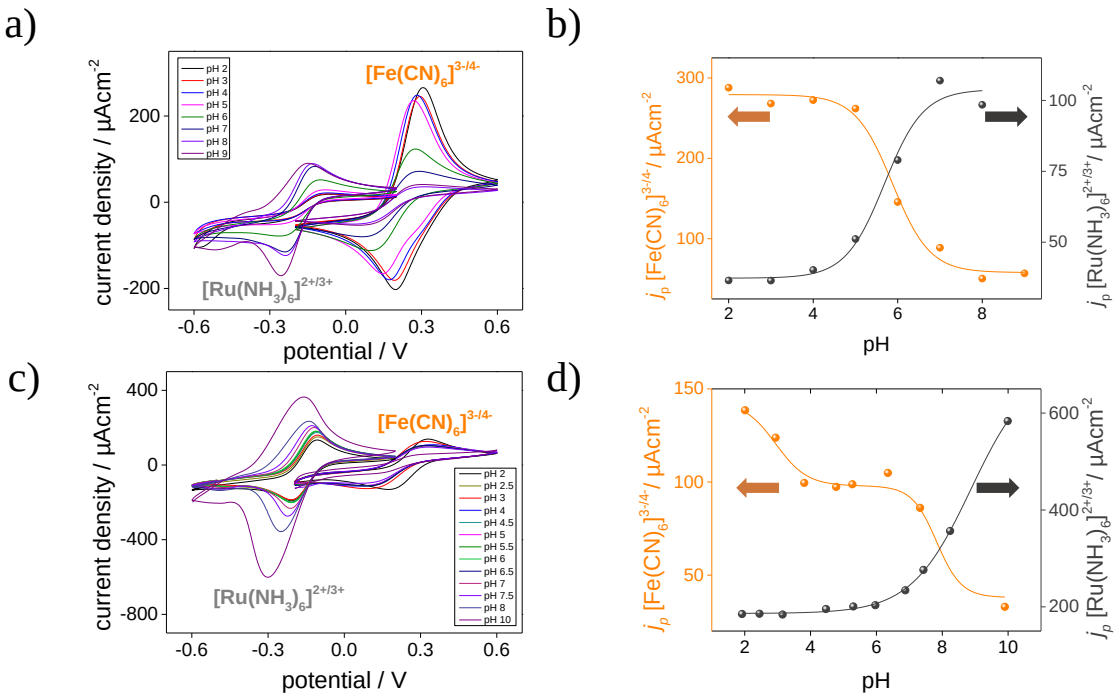

Figure 5